

# Ethylene Epoxidation Activity Over Ag-Based Catalysts on Different Nanocrystalline Perovskite Titanate Supports

Atiporn Chongterdtoonskul · Johannes W. Schwank ·  
Sumaeth Chavadej

Received: 16 February 2012/Accepted: 28 May 2012/Published online: 19 June 2012  
© Springer Science+Business Media, LLC 2012

**Abstract** Ag-based catalysts on different nanocrystalline perovskite supports ( $\text{MgTiO}_3$ ,  $\text{CaTiO}_3$ ,  $\text{SrTiO}_3$ , and  $\text{BaTiO}_3$ ), and nanocrystalline  $\text{TiO}_2$  support prepared by a sol–gel method and on a commercial  $\alpha\text{-Al}_2\text{O}_3$  support were comparatively studied for catalytic activity of the ethylene epoxidation reaction. The dependence of ethylene oxide production performance on calcination temperature of the support, type of titanate nanocrystal supports, Ag loading, and reaction temperature was systematically investigated. The catalysts were analytically characterized by a Brunauer–Emmett–Teller (BET) surface area, X-ray diffraction (XRD), field emission scanning electron microscopy (FE-SEM), transmission electron microscopy (TEM), energy-dispersive X-ray spectroscopy (EDS), temperature programmed desorption (TPD), and X-ray photoelectron spectroscopy (XPS). Among studied catalysts, the 17.2 wt% Ag/ $\text{SrTiO}_3$  catalyst exhibited the highest catalytic activity towards ethylene epoxidation reaction.

**Keywords** Perovskite supports ·  $\text{SrTiO}_3$  · Nanocrystalline  $\text{TiO}_2$  · Sol–gel · Ethylene epoxidation

---

A. Chongterdtoonskul · S. Chavadej (✉)  
The Petroleum and Petrochemical College, Chulalongkorn University, Soi Chula 12, Phyathai Road, Pathumwan, Bangkok 10330, Thailand  
e-mail: sumaeth.c@chula.ac.th

J. W. Schwank  
Department of Chemical Engineering, University of Michigan, Ann Arbor, MI 48109, USA

S. Chavadej  
Center of Excellence on Petrochemical and Materials Technology, Chulalongkorn University, Bangkok 10330, Thailand

## 1 Introduction

Silver-catalyzed ethylene epoxidation to produce ethylene oxide (EO), a key intermediate in the chemical industry, is an industrially applied heterogeneous catalytic process. A number of significant efforts have been made to improve the catalysts used in this process since the discovery of this reaction by Lefort [1]. The active phase of silver catalysts, the mechanism of this reaction, and the effect of promoters have been intensively investigated [2–16]. Ayame et al. [17] synthesized pure crystalline  $\alpha\text{-Al}_2\text{O}_3$  carriers used in catalytic epoxidation from primary  $\alpha\text{-Al}_2\text{O}_3$  crystal particles. The carriers had high purity with homogeneous pore distribution and the pores comprised spaces or cavities surrounded by crystal planes of the primary particles. The Ag catalysts supported on the  $\alpha\text{-Al}_2\text{O}_3$  crystal carriers were found to exhibit good catalytic performance i.e. high and very stable ethylene conversion and ethylene oxide selectivity in the ethylene epoxidation reaction without added organic halides. In 2007, Fotopoulos and Triantafyllidis [18] compared the ethylene epoxidation performance of Ag catalysts supported on non-porous  $\text{SiO}_2$ , microporous silicalite zeolite, and MCM-41 and HMS mesoporous silicates to conventional low surface area  $\alpha\text{-Al}_2\text{O}_3$ . The Ag catalysts supported on MCM-41 and HMS mesoporous silicates were found to be active in ethylene epoxidation reaction, providing EO selectivity similar to or slightly lower than those of the Ag catalysts supported on non-porous  $\text{SiO}_2$  and conventional low surface area  $\alpha\text{-Al}_2\text{O}_3$  at a relatively low temperature ( $\sim 503$  K). Particularly, one of the most interesting developments for catalysis is the modification of the surface structure and electronic properties of nanoparticles [19]. These characteristics determine the features of the interaction of reactants with active sites, reactivity of adsorbed species, and structure so they directly affect the

activity and selectivity of nano-systems in heterogeneous catalysis.

Furthermore, a number of researchers have extensively investigated new preparation methods, i.e. deposition–precipitation, atomic layer deposition, etc., to improve the performance of catalysts for individual reactions [20, 21]. Kim et al. [22] compared several preparation methods for  $\alpha$ -Al<sub>2</sub>O<sub>3</sub> supported Ag catalysts i.e. precipitation, modified precipitation, water–alcohol, and microemulsion methods. Among all the preparation methods, the catalysts prepared by a water–alcohol method had higher activities for the ethylene oxide than those prepared by a microemulsion method. This might be due to the larger particle sizes (about 30 nm) as well as easier desorption of the molecular oxygen from the catalysts. They also found that the Ag particles of about 30 nm (catalysts prepared by modified precipitation and water–alcohol methods) showed better stability and higher activity than the particles smaller than 15 nm (catalysts prepared by precipitation and microemulsion methods).

One of the most promising catalyst preparation methods is sol–gel. The sol–gel process has emerged as an effective technique for the synthesis of noble metal–dielectric nanocomposites with enhanced nonlinear optical properties. The advantages of the sol–gel process are high homogeneity of the starting solutions in the molecular scale, low processing temperatures, and the possibility of incorporating many different metal dopants into different matrixes, leading to a variety of synthesized materials for various applications [23, 24]. Furthermore, Puangpatch et al. [25] proved that the nanocrystalline structures with a high pore uniformity of SrTiO<sub>3</sub> were active for photocatalytic water splitting. Recently, they compared the photocatalytic H<sub>2</sub> production performance on different types of perovskite titanate nanocrystal photocatalysts (MgTiO<sub>3</sub>, CaTiO<sub>3</sub>, and SrTiO<sub>3</sub>). The experimental results showed that the 0.5 wt% Pt-loaded SrTiO<sub>3</sub> nanocrystals synthesized by a single-step sol–gel method and calcined at 923 K exhibited the highest photocatalytic H<sub>2</sub> production activity [26].

In our previous work [27], the effects of various oxide supports (Al<sub>2</sub>O<sub>3,Acid</sub>, Al<sub>2</sub>O<sub>3</sub> C,  $\alpha$ -Al<sub>2</sub>O<sub>3</sub>, SiO<sub>2</sub>, and SrTiO<sub>3</sub>) for Ag catalysts on EO selectivity and yield were investigated. The Ag supported on SrTiO<sub>3</sub> was found to be the most effective catalyst for epoxidation of ethylene, giving unusually high EO selectivity up to 99 % and a yield of 4.5 %. With a continuation of the achievement of the perovskite SrTiO<sub>3</sub> nanocrystal catalyst development, the purpose of this present work was to investigate the catalytic EO activity of Ag-based catalysts on various nanocrystalline perovskite titanate supports. Various nanocrystal perovskite titanates and TiO<sub>2</sub> synthesized via the sol–gel method with the aid of a structure-directing surfactant were

used as a Ag support for the ethylene epoxidation reaction. Moreover, the catalytic performance of each studied catalyst was correlated with its physical properties.

## 2 Experimental

### 2.1 Materials

$\alpha$ -Al<sub>2</sub>O<sub>3</sub> with a specific surface area of 0.109 m<sup>2</sup>/g was supplied by Fluka. Silver nitrate (AgNO<sub>3</sub>) was supplied by S.R. Lab. Tetraisopropyl orthotitanate (TIPT, Ti(OCH(CH<sub>3</sub>)<sub>2</sub>)<sub>4</sub>), magnesium nitrate hexahydrate (Mg(NO<sub>3</sub>)<sub>2</sub>·6H<sub>2</sub>O), calcium nitrate tetrahydrate (Ca(NO<sub>3</sub>)<sub>2</sub>·4H<sub>2</sub>O), strontium nitrate (Sr(NO<sub>3</sub>)<sub>2</sub>), barium nitrate (Ba(NO<sub>3</sub>)<sub>2</sub>), and laurylamine (LA, CH<sub>3</sub>(CH<sub>2</sub>)<sub>11</sub>NH<sub>2</sub>) were purchased from Merck. Acetylacetone (ACA, CH<sub>3</sub>COCH<sub>2</sub>COCH<sub>3</sub>) was obtained from S.D. Fine-Chemical. Hydrochloric acid (HCl) and ethanol (C<sub>2</sub>H<sub>5</sub>OH) were purchased from Labscan. All chemicals used were analytical grade and used as received without further purification.

### 2.2 Catalyst Preparation Procedures

A nanocrystalline TiO<sub>2</sub> support was synthesized via the sol–gel process with surfactant-assisted template in a TIPT/LA modified with an ACA system [24, 28–33]. ACA was first mixed with TIPT at a molar ratio of 1:1. Then, the mixed TIPT/ACA solution was gently shaken until homogeneous mixing. A quantity of 60 ml of distilled water and 0.5 ml of HCl were added consecutively in a separate beaker, followed by the LA surfactant to obtain 0.1 M of LA. Afterwards, the mixture was stirred until a clear solution was obtained. Next, the LA solution was added to the ACA-modified TIPT solution. The resultant mixture was continuously stirred to obtain a homogeneously transparent sol. Then, the sol-containing solution was placed in an oven at 353 K for a week in order to obtain complete gel formation. Subsequently, the gel was further dried at 353 K for 2 days to eliminate the remaining solvent which was mainly the distilled water used in the preparation of the LA solution. The dried gel was finally calcined at 923 K to remove the LA surfactant and to subsequently produce the desired nanocrystalline TiO<sub>2</sub> support.

The nanocrystalline perovskite titanates (MgTiO<sub>3</sub>, Ca-TiO<sub>3</sub>, SrTiO<sub>3</sub>, and BaTiO<sub>3</sub>) were also synthesized by the same sol–gel process with the aid of a structure-directing surfactant as used for the synthesis of the TiO<sub>2</sub> support [25, 26, 34, 35]. Firstly, the TIPT and ACA at an equimolar ratio were mixed together. The mixed TIPT/ACA solution was gently shaken until a homogeneous mixture was achieved. An appropriate amount of corresponding alkaline earth nitrate (Mg(NO<sub>3</sub>)<sub>2</sub>·6H<sub>2</sub>O, Ca(NO<sub>3</sub>)<sub>2</sub>·4H<sub>2</sub>O, Sr(NO<sub>3</sub>)<sub>2</sub>

or  $\text{Ba}(\text{NO}_3)_2$  was dissolved in distilled water. Next, ethanol was mixed with the as-prepared alkaline earth nitrate solution. After that, 1.112 g of the LA surfactant and 0.5 ml of HCl were added to obtain the alkaline earth nitrate/LA/HCl solution. The alkaline earth nitrate/LA/HCl solution was poured into the TiPT/ACA solution, based on the alkaline earth metal-to-Ti molar ratio of 1:1 and the LA-to-(alkaline earth metal + Ti) ratio of 0.25:1. The final mixture was continuously stirred at room temperature until a homogeneous transparent sol was obtained. Then, the sol-containing solution was placed in an oven at 353 K for 4 days to achieve complete gelation. Afterwards, the gel was further dried at 353 K for 4 days to eliminate the solvents. Finally, the dried gel was calcined at 923 K (the calcination temperature of all synthesized supports was performed only at 923 K because the highest catalytic activity was found on the  $\text{SrTiO}_3$  support at that temperature, as described later in Sect. 3.2.1) to produce the desired nanocrystalline perovskite titanate supports.

All Ag-based catalysts on different synthesized nanocrystalline perovskite titanates ( $\text{MgTiO}_3$ ,  $\text{CaTiO}_3$ ,  $\text{SrTiO}_3$ , and  $\text{BaTiO}_3$ ),  $\text{TiO}_2$  and  $\alpha\text{-Al}_2\text{O}_3$  were prepared by incipient wetness impregnation. The nanocrystalline perovskite titanates and  $\alpha\text{-Al}_2\text{O}_3$  supports were impregnated with an aqueous silver nitrate solution to achieve different nominal Ag loadings of 12.5, 15, 17.5, and 20 wt%. After the impregnation step, the catalysts were dried at 383 K overnight, followed by calcination in air at 773 K for 5 h.

### 2.3 Catalyst Characterization Techniques

The crystallinity of the synthesized catalysts was examined by an X-ray diffractometer (XRD, Rigaku, RINT 2200 HV) equipped with a Ni filter and a Cu  $\text{K}\alpha$  radiation source ( $\lambda = 1.542 \text{ \AA}$ ) operating at 40 kV and 30 mA. The catalyst samples were scanned using a continuous scanning mode at a rate of  $5^\circ \text{ min}^{-1}$  in the range of  $2\theta$  from  $5^\circ$  to  $90^\circ$ . The Ag crystallite size ( $D$ ) was calculated from the line broadening of the corresponding X-ray diffraction peak of Ag using the Debye–Scherer equation [36, 37] with the full line width at half maximum of intensity and the  $2\theta$  value, as follows:

$$D = \frac{0.9\lambda}{B \cos \theta}$$

where  $\lambda$  is the x-ray wavelength (1.542  $\text{\AA}$  for Cu source),  $B$  is the full width at half maximum (FWHM) of the diffraction peak measured at  $2\theta$ , and  $\theta$  is the diffraction angle.

The actual contents of the Ag loaded on the catalyst samples were analyzed by an atomic absorption spectrophotometer (AAS, Varian, Spectr AA-300). The  $\text{N}_2$  adsorption–desorption isotherms were obtained by a Brunauer–Emmett–Teller (BET) surface area analyzer

(Quantachrome, SAA-1MP) to determine the specific surface areas of all synthesized catalyst samples. Prior to analysis, each catalyst sample was outgassed at 473 K for 8 h.

The surface morphology of the studied catalysts was observed by a field emission scanning electron microscope (FE-SEM, JEOL 5200-2AE). Before the examination, the samples were coated with Pt to improve their conductivity. The catalyst morphologies and particle sizes of the loaded Ag were examined by transmission electron microscopy (TEM, JEOL 3011 at 300 kV and JEOL 2010 at 200 kV). The specimens for the TEM analysis were prepared by ultrasonically dispersing powders of the catalysts in ethanol and then placing drops of the suspension onto a Cu grid coated with a carbon film. An energy dispersive X-ray spectrometer (EDS) attached to the TEM was used to verify the existence of Ag particles on the different supports. The Ag particle sizes were determined from statistical analysis of the diameters of particles obtained from the TEM images.

The oxygen and ethylene adsorption capabilities of the catalysts were obtained using a temperature-programmed desorption (TPD) analyzer (Quantachrome, Chembet 3000). For the TPD experiments, oxygen (4.99 %  $\text{O}_2$  in He) or pure ethylene (99.99 %  $\text{C}_2\text{H}_4$ ) was allowed to adsorb onto the catalyst surface at 473 K for 2 h. After that, the catalyst samples were cooled to room temperature in a stream of high-purity He. The catalyst samples were then heated from room temperature to 1,173 K with a heating rate of 10 K/min, and the desorbed gas was swept by the high-purity He at a flow rate of 20  $\text{cm}^3/\text{min}$ . The desorption profile of either oxygen or ethylene present in the effluent stream was measured by a thermal conductivity detector (TCD).

The oxidation state of the supported Ag particles on different supports was analyzed by an X-ray photoelectron spectrometer (XPS, Shimadzu, Kratos). A monochromatic Al  $\text{K}\alpha$  source was used as the X-ray source. The relative surface charging of the samples was corrected by referencing all the energies to the C1s level as an internal standard at 284.8 eV [38]. A thermogravimetric-differential thermal analyzer (TG-DTA, PerkinElmer, Pyris Diamond) was used to quantify the amount of coke deposited on the spent catalysts [39, 40].

### 2.4 Activity Testing Experiments

The catalytic ethylene epoxidation activities over different synthesized catalysts were performed in a packed-bed 8-mm ID tubular reactor under 24.7 psia with different reaction temperatures. A 30 mg packed catalyst was initially pretreated with oxygen at 473 K for 2 h in order to diminish all impurities and to remove residual moisture from the

catalyst. The feed gas was a mixture of 40 % ethylene in He, pure oxygen (HP grade), and pure helium (HP grade). The flow rates of these gas streams were regulated by mass flow controllers to achieve a feed gas composition of 6 % ethylene and 6 % oxygen with a helium balance. The feed gas was passed through the reactor at a constant space velocity of 6,000 h<sup>-1</sup>, and the reaction temperature was varied from 498 to 563 K for all catalysts. The compositions of the feed and product gases were analyzed by using an on-line gas chromatograph (Perkin Elmer, ARNEL) equipped with a 60/80 CARBOXEN 1 packed column (capable of separating carbon monoxide, carbon dioxide, ethylene, and oxygen) and a Rt-U PLOT capillary column (capable of separating EO, ethane, and propane). The CO concentration was neglected under the studied conditions because it was below the detectable limit. The formation of acetaldehyde was not detected because it was further oxidized to carbon dioxide and water so it appeared only in trace amounts (below the detectable limit) [41]. The measured amount CO<sub>2</sub> came from the oxidation of ethylene, EO and further oxidation of acetaldehyde. The catalytic activities of all catalysts at 6 h of operation were used for comparisons. Moreover, the catalytic system was operated up to 48 h over the best two Ag-based catalysts and the Ag on commercial  $\alpha$ -Al<sub>2</sub>O<sub>3</sub> catalyst to observe the long-term stability of these catalysts.

### 3 Results and Discussion

#### 3.1 Catalyst Characterization Results

##### 3.1.1 XRD Results

Figure 1 shows the XRD patterns of Ag/SrTiO<sub>3</sub> catalysts with various Ag loadings. Compared with the pristine SrTiO<sub>3</sub>, all the Ag-loaded ones were found to exhibit the similar highly crystalline structure, which refers to the single phase of cubic perovskite-type SrTiO<sub>3</sub> [34]. The dominant peaks of metallic silver at 2 $\theta$  of about 28°, 38°, and 44° correspond to (110), (111), and (200) planes, respectively. On the other hand, there was the presence of an extremely small Ag<sub>2</sub>O peak at 2 $\theta$  of 35° which was also previously observed for the SrTiO<sub>3</sub> calcined at 773 K [42]. The XRD results reveal that the Ag catalyst on the SrTiO<sub>3</sub> support was mostly in metallic form which is in good agreement with our previous work [27]. The XRD patterns of Ag catalysts on different perovskite titanate supports at their optimum Ag loadings (corresponding to their highest catalytic activities towards ethylene epoxidation reaction) are comparatively shown in Fig. 2. All of the Ag/nano-crystalline cubic perovskite titanate catalysts (Ag/MgTiO<sub>3</sub>, Ag/CaTiO<sub>3</sub>, Ag/SrTiO<sub>3</sub>, and Ag/BaTiO<sub>3</sub>) showed higher crystalline structures than that of the Ag/TiO<sub>2</sub> catalyst.

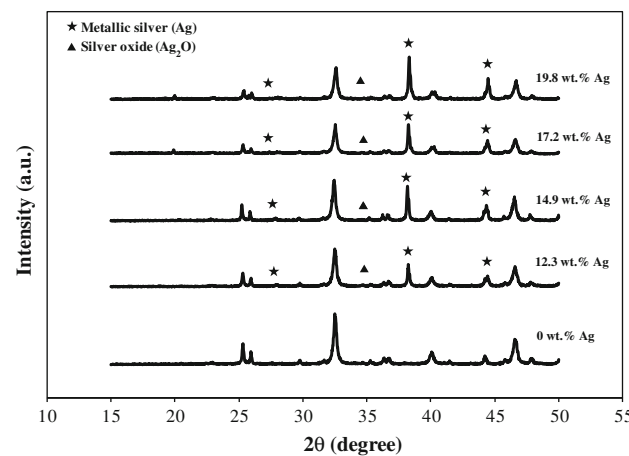


**Fig. 1** XRD patterns of Ag/SrTiO<sub>3</sub> catalysts with various Ag loadings. The SrTiO<sub>3</sub> support was calcined at 923 K, followed by Ag impregnation and a second calcination at 773 K

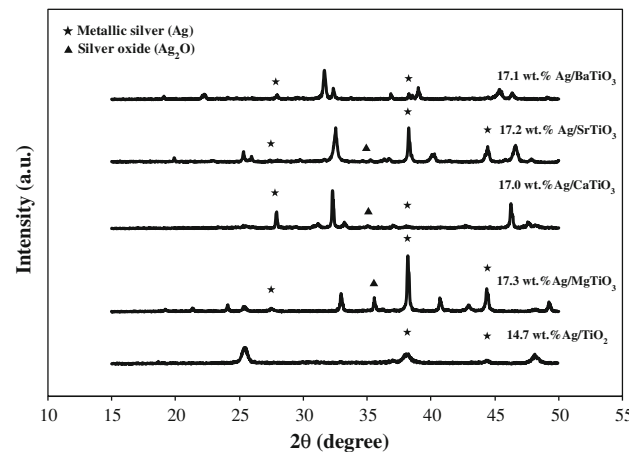


**Fig. 2** XRD patterns of Ag catalysts on different supports at their optimum Ag loadings. The SrTiO<sub>3</sub> support was calcined at 923 K, followed by Ag impregnation and a second calcination at 773 K

Moreover, only the Ag/MgTiO<sub>3</sub> catalyst showed a clear Ag<sub>2</sub>O peak. The XRD results suggest that the Ag-loaded on various supports is mostly in the metallic form, except the MgTiO<sub>3</sub> exhibiting a significant amount of Ag<sub>2</sub>O.

##### 3.1.2 Specific Surface Area Results

As shown in Table 1, the specific surface area of the unloaded SrTiO<sub>3</sub> decreases from 6 to 1.9 m<sup>2</sup>/g with increasing calcination temperature from 673 to 1,073 K. The reduction in the specific surface area of the Ag unloaded SrTiO<sub>3</sub> with increasing calcination temperature is according to the pore collapse, relating to the crystallization of the walls separating the mesopores. Indeed, phase transformation and sintering might be involved [43]. As shown in Table 2, among the Ag catalysts on different supports calcined at 923 K, the specific surface area of Ag-

**Table 1** Characteristics of the 17.5 wt% Ag catalysts on SrTiO<sub>3</sub> supports at various support calcination temperatures

Support calcination temperature (K)	Specific surface area (m <sup>2</sup> /g)	Ag particle size <sup>a</sup> (nm)	Ag crystallite size <sup>b</sup> (nm)
673	4.7 (6.0) <sup>c</sup>	53.4 ± 0.5	50.1
773	3.0 (4.4) <sup>c</sup>	58.6 ± 0.5	52.1
873	1.9 (3.1) <sup>c</sup>	57.2 ± 0.5	54.3
923	1.5 (2.8) <sup>c</sup>	59.4 ± 0.5	57.3
973	1.4 (2.3) <sup>c</sup>	61.6 ± 0.5	64.4
1,073	1.2 (1.9) <sup>c</sup>	65.9 ± 0.5	69

<sup>a</sup> From TEM analysis<sup>b</sup> From XRD analysis<sup>c</sup> Specific surface area of support without Ag loading

based catalysts on the BaTiO<sub>3</sub> support is the lowest one, followed by the Ag/SrTiO<sub>3</sub> catalyst. However, the specific surface area of the TiO<sub>2</sub>-supported catalyst was much higher than those of all perovskite titanate supports.

### 3.1.3 Surface Morphology

From the surface morphologies of the 17.5 wt% Ag-loaded on SrTiO<sub>3</sub> supports calcined at different temperatures, it can be clearly seen that the particles of the SrTiO<sub>3</sub> support become larger as the calcination temperature increased (Fig. 3). These results correspond well with the specific surface area results. As will be discussed later, the 17.2 wt% Ag catalyst on the SrTiO<sub>3</sub> support calcined at 923 K provided the highest catalytic performance of the ethylene epoxidation reaction. Thus, this present work focused on this calcination temperature for all other supports. The surface morphologies of the Ag catalysts on different supports before the reaction (Fig. 4) were compared to those after the reaction (Fig. 5). As mentioned before, the XRD results showed the presence of loaded Ag mostly in metallic form on all studied supports. The SEM images also confirm the existence of the cubic perovskite-type of the synthesized MgTiO<sub>3</sub>, CaTiO<sub>3</sub>, SrTiO<sub>3</sub>, and BaTiO<sub>3</sub>. The SEM images with the EDS also showed good distribution of nanosized Ag particles on all the supports. After the reaction, a change in surface topology of the catalysts was clearly observed, especially for the Ag/BaTiO<sub>3</sub> catalyst (see Figs. 4e, 5e). The Ag particles on all supports tended to agglomerate and became larger due to catalyst sintering during the reaction. It increased from 44 to 48 nm for Ag/TiO<sub>2</sub>; from 57 to 59 nm for Ag/MgTiO<sub>3</sub>; from 53 to 57 nm for Ag/CaTiO<sub>3</sub>; from 59 to 64 nm for Ag/SrTiO<sub>3</sub>; and from 53 to 61 nm for Ag/BaTiO<sub>3</sub>.

Table 1 shows the effect of the calcination temperature of the SrTiO<sub>3</sub> support on the Ag crystallite size and particle

size at the optimum Ag loading of 17.5 wt% (providing the highest EO activity [27]). As the support calcination temperature increased, both crystalline and particle sizes of Ag became larger, whereas the specific surface area of the SrTiO<sub>3</sub> support decreased markedly. This is possibly because the calcination temperature of the support may alter the physical properties of the support surface [33]. Interestingly, for any support calcination temperature, the crystallite size was close to the particle size, suggesting that this preparation technique can produce single nanosize crystalline Ag particles in the range of 50–70 nm.

Table 2 shows the specific surface area, particle size and crystallite size of Ag loaded on different titanate supports at their optimum Ag loadings towards their highest catalytic ethylene epoxidation activities. The prepared Ag catalysts on all studied titanate supports had single crystalline particles. The SrTiO<sub>3</sub> support provided the largest Ag particle size as compared with the other supports.

The existence of Ag nanoparticles on all the supports was verified by the TEM/EDS technique. The inhomogeneous dispersion of Ag nanoparticles throughout the different supports is displayed in Fig. 6. The Ag particle sizes on the studied SrTiO<sub>3</sub> supports at different calcination temperatures (Table 1) became larger when the calcination temperature increased. The largest Ag particle size of about 66 nm was obtained from the SrTiO<sub>3</sub> support calcined at 1,073 K. Furthermore, the average sizes of Ag nanoparticles in all the titanate catalysts are summarized in Table 2. The largest average Ag particle size (59 nm) was found on the SrTiO<sub>3</sub> support, while the smallest average Ag particle size (44 nm) was found on the TiO<sub>2</sub> support. The particle sizes observed from the TEM images were found to be close to the crystallite sizes obtained from the XRD analysis. Both TEM and XRD results verify that the synthesis technique used in this study could provide the single crystalline structure of Ag particles on all studied supports.

### 3.1.4 TPD Results

Temperature programmed desorption can be used to investigate the interaction between oxygen or ethylene and a catalyst surface with respect to temperature as calculated in terms of the uptakes of oxygen and ethylene which are involved in the ethylene epoxidation in the present study. Table 3 shows the ethylene and oxygen uptakes for all studied catalysts in the temperature range of 400–700 K in which the EO formation was found to occur in this temperature range (more EO was formed than the complete oxidation to produce CO<sub>2</sub>). The ethylene uptakes were comparably high for all titanate supports, except the TiO<sub>2</sub> support and the highest ethylene uptake was found on the 17.2 wt% Ag/SrTiO<sub>3</sub> catalyst. Hence, the epoxidation of ethylene is an O<sub>2</sub>-controlled reaction. It can be clearly seen

**Table 2** Characteristics of Ag catalysts on different titanate supports at their own optimum Ag loadings (corresponding to the highest ethylene epoxidation activity)

Support	Actual Ag loading (wt%)	Specific surface area ( $\text{m}^2/\text{g}$ )	Ag particle size <sup>a</sup> (nm)	Ag crystallite size <sup>b</sup> (nm)
$\text{TiO}_2$	14.7	28.6 (36.7) <sup>c</sup>	$44.4 \pm 0.5$	43.2
$\text{MgTiO}_3$	17.3	16.7 (29.4) <sup>c</sup>	$56.5 \pm 0.6$	55.9
$\text{CaTiO}_3$	17.0	3.5 (12.8) <sup>c</sup>	$52.6 \pm 0.6$	54.3
$\text{SrTiO}_3$	17.2	1.5 (2.8) <sup>c</sup>	$59.4 \pm 0.5$	57.3
$\text{BaTiO}_3$	17.1	1.1 (2.4) <sup>c</sup>	$53.2 \pm 0.5$	54.6

<sup>a</sup> From TEM analysis

<sup>b</sup> From XRD analysis

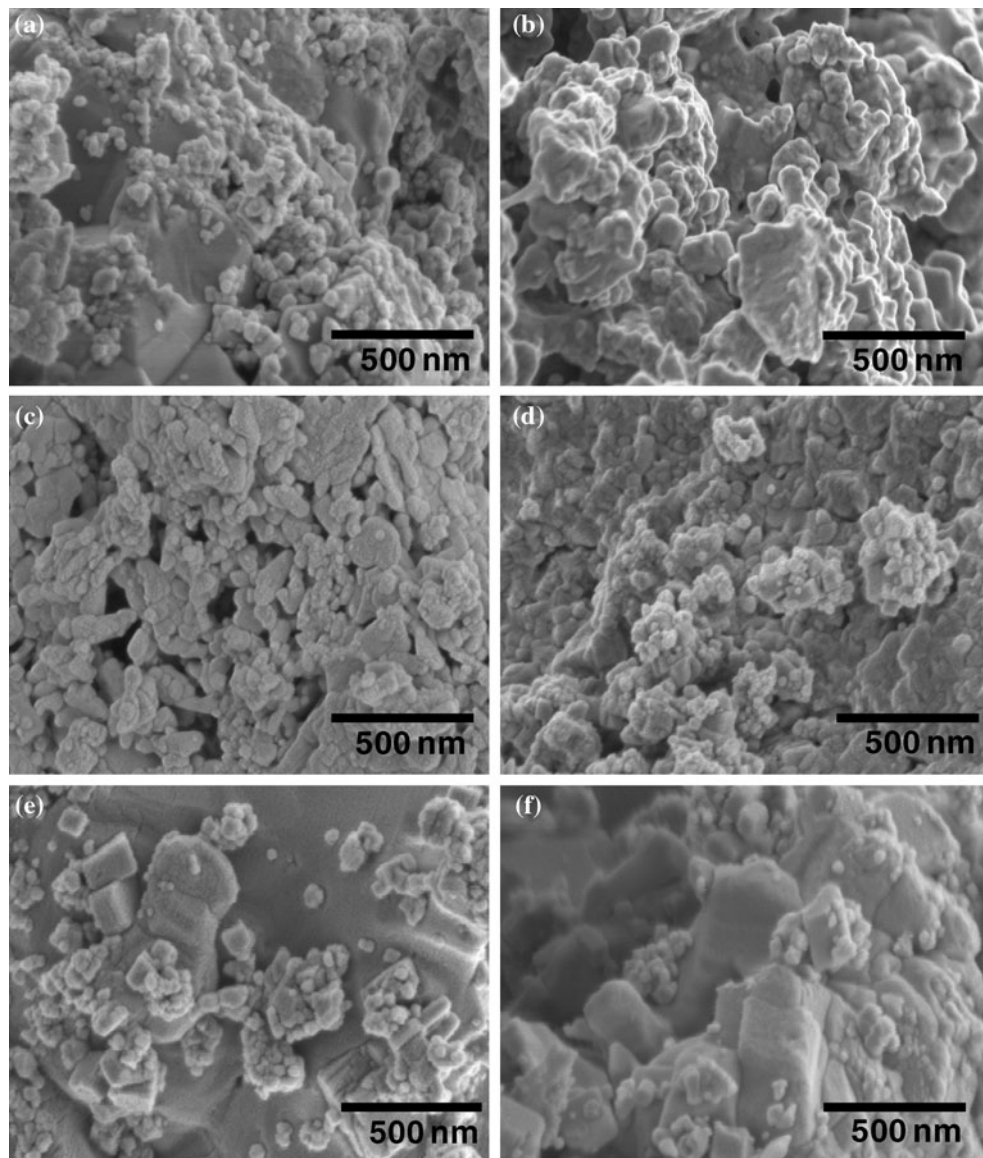
<sup>c</sup> Specific surface area of support without Ag loading

that the oxygen uptake for the pristine  $\text{SrTiO}_3$  support substantially increased after Ag loading, whereas the ethylene uptake slightly increased. Moreover, the largest oxygen and ethylene uptakes were obtained on the 17.2 wt% Ag/ $\text{SrTiO}_3$  catalyst corresponding to the highest catalytic activity towards EO formation, implying that both oxygen and ethylene storage on the catalyst surface plays a major role for the ethylene epoxidation reaction which will be discussed later.

### 3.1.5 XPS Results

The existence of both metallic silver (Ag) and silver oxide ( $\text{Ag}_2\text{O}$ ) of the loaded Ag on the  $\text{SrTiO}_3$  support before and

**Fig. 3** SEM images of 17.5 wt% Ag/ $\text{SrTiO}_3$  catalysts at various support calcination temperatures of supports, **a** 673 K, **b** 773 K, **c** 873 K, **d** 923 K, **e** 973 K, and **f** 1,073 K ( $\times 70,000$ ), followed by Ag impregnation and final calcination at 773 K



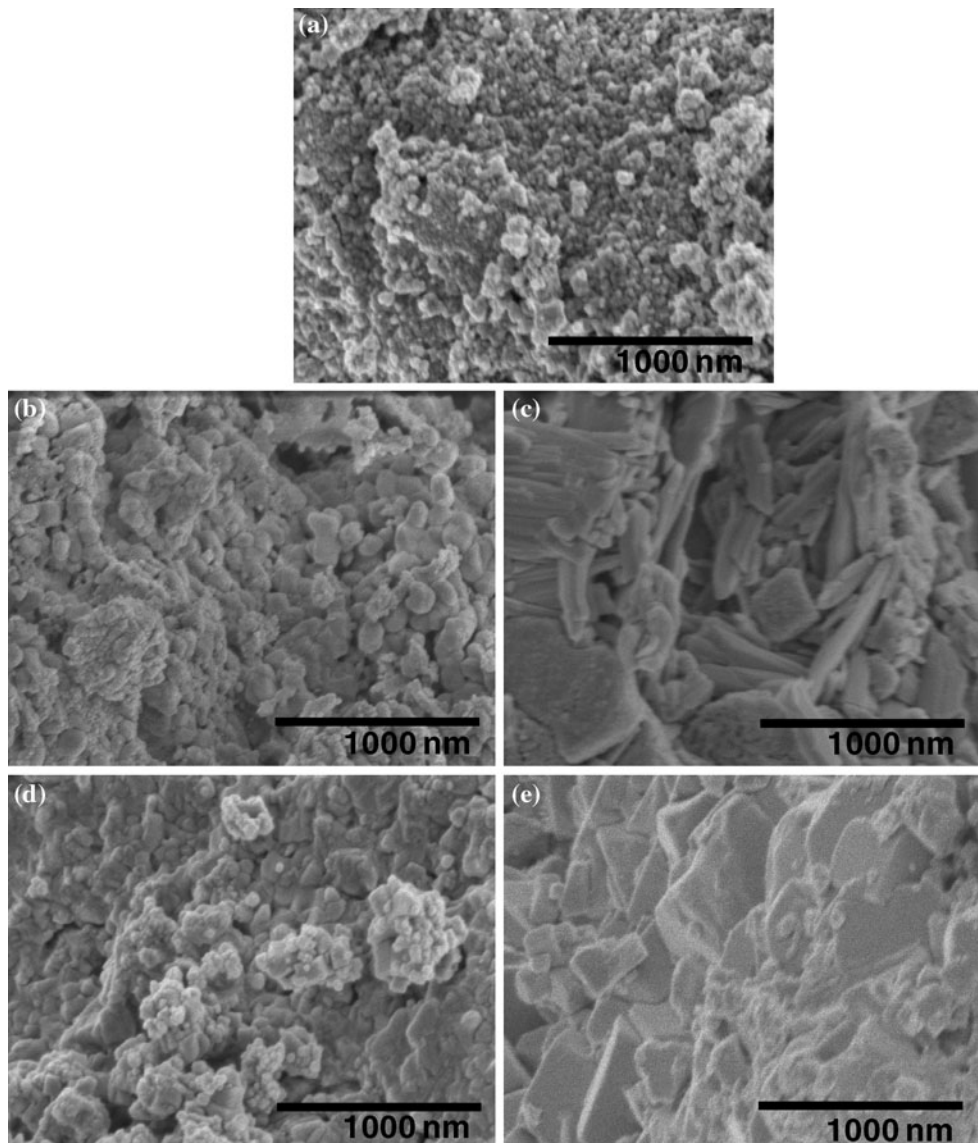


**Fig. 4** SEM images of Ag catalysts prepared by sol–gel method on different supports before the reaction, **a** 14.7 wt% Ag/TiO<sub>2</sub>, **b** 17.3 wt% Ag/MgTiO<sub>3</sub>, **c** 17.0 wt% Ag/CaTiO<sub>3</sub>, **d** 17.2 wt% Ag/SrTiO<sub>3</sub>, and **e** 17.1 wt% Ag/BaTiO<sub>3</sub> catalysts ( $\times 50,000$ )

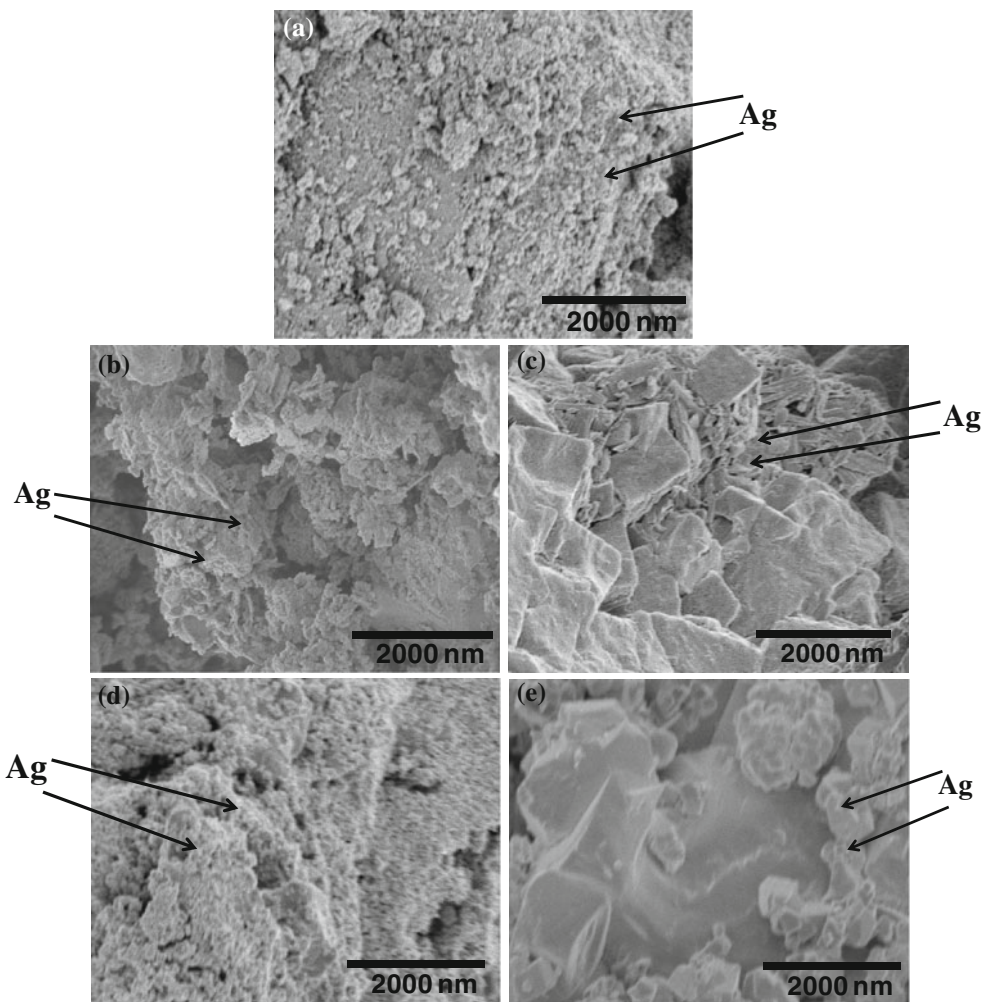
after the reaction were verified by the deconvoluted XPS spectra (Fig. 7). The two dominant peaks with their centers at 367.5 and 373.5 eV, corresponding to the Ag 3d<sub>5/2</sub> and Ag 3d<sub>3/2</sub> levels, respectively indicate the formation of metallic Ag. The small doublet peaks appeared at 366.5 and 371.5 eV of Ag<sub>2</sub>O 3d<sub>5/2</sub> and Ag<sub>2</sub>O 3d<sub>3/2</sub>, respectively confirm the formation of Ag<sub>2</sub>O [38]. The XPS results suggest that the synthesized Ag catalyst on the SrTiO<sub>3</sub> support mostly contained metallic Ag. For the 17.2 wt% Ag/SrTiO<sub>3</sub> catalyst, the ratio of Ag to Ag<sub>2</sub>O increased from 9.5 before the reaction to 13.3 after the reaction, indicating that a significant portion of the Ag<sub>2</sub>O was reduced to metallic Ag during the reaction. According to the lean O<sub>2</sub>

reaction condition used in this study, the further oxidation of EO to CO<sub>2</sub> was hampered.

### 3.1.6 TG-DTA Results

Table 4 summarizes the amount of coke formation on the spent Ag-loaded catalysts after the ethylene epoxidation reaction for 6 and 48 h. The highest coke formation (9.2 % at 6 h and 15.7 % at 48 h) was found on the 17.3 wt% Ag/MgTiO<sub>3</sub> catalyst while the 17.1 wt% Ag/BaTiO<sub>3</sub> catalyst had the lowest amount of coke at 6 h of operation (2.5 %) and the 17.2 wt% Ag/SrTiO<sub>3</sub> catalyst had the lowest amount of coke at 48 h of operation (4.5 %).

**Fig. 5** SEM images with the EDS of spent Ag catalysts on different supports after the reaction, **a** 14.7 wt% Ag/TiO<sub>2</sub>, **b** 17.3 wt% Ag/MgTiO<sub>3</sub>, **c** 17.0 wt% Ag/CaTiO<sub>3</sub>, **d** 17.2 wt% Ag/SrTiO<sub>3</sub>, and **e** 17.1 wt% Ag/BaTiO<sub>3</sub> catalysts ( $\times 20,000$ )



The relation of coke formation and the catalytic activity towards EO formation will be further discussed later.

### 3.2 Ethylene Epoxidation Activity Results

#### 3.2.1 Effect of Support Calcination Temperature

According to our previous work [27], the SrTiO<sub>3</sub> support was, for the first time, used as a Ag catalyst and the 17.2 wt% Ag loading was found to provide the best catalytic activity in terms of EO selectivity and EO yield. This catalyst provided both the highest EO yield at 4.5 % and maximum EO selectivity up to 99 %. As a result, the Ag-based SrTiO<sub>3</sub> catalyst was further studied in the present work in order to improve yield and selectivity for EO production. First, the support calcination temperature was varied from 673 to 1,073 K with the fixed calcination temperature of Ag loading at 773 K and the Ag loading of about 17.2 wt%. The effect of the support calcination temperature on EO selectivity and yield is shown in Fig. 8. The SrTiO<sub>3</sub> support calcined at 923 K gave the best

catalytic performance with the highest EO yield of 4.7 % and EO selectivity of 99.1 %. It can be clearly seen that the activity dropped sharply after the calcination temperature further increased from 923 to 973 K. The improved performance of the 17.2 wt% Ag/SrTiO<sub>3</sub> catalyst at this support calcination temperature of 923 K may be attributed to the appropriate specific surface area that is suitable for the reaction and/or the Ag particle size. A decrease in the specific surface area simply reduces the reaction sites, resulting in lowering undesired reactions especially deep oxidation. However, a very high support calcination temperature may make the specific surface area too small to provide the necessary reaction sites. The results also confirm that the ethylene epoxidation reaction seems to favor over low-surface-area catalysts. The optimum support calcination temperature was 923 K for all supports (MgTiO<sub>3</sub>, CaTiO<sub>3</sub>, SrTiO<sub>3</sub>, and BaTiO<sub>3</sub>), except for TiO<sub>2</sub> which the optimum calcination temperature was found to be 873 K. However, the catalytic activity for other catalysts was substantially lower than the Ag/SrTiO<sub>3</sub> catalyst (best catalyst). Thus, the same temperature of 923 K which

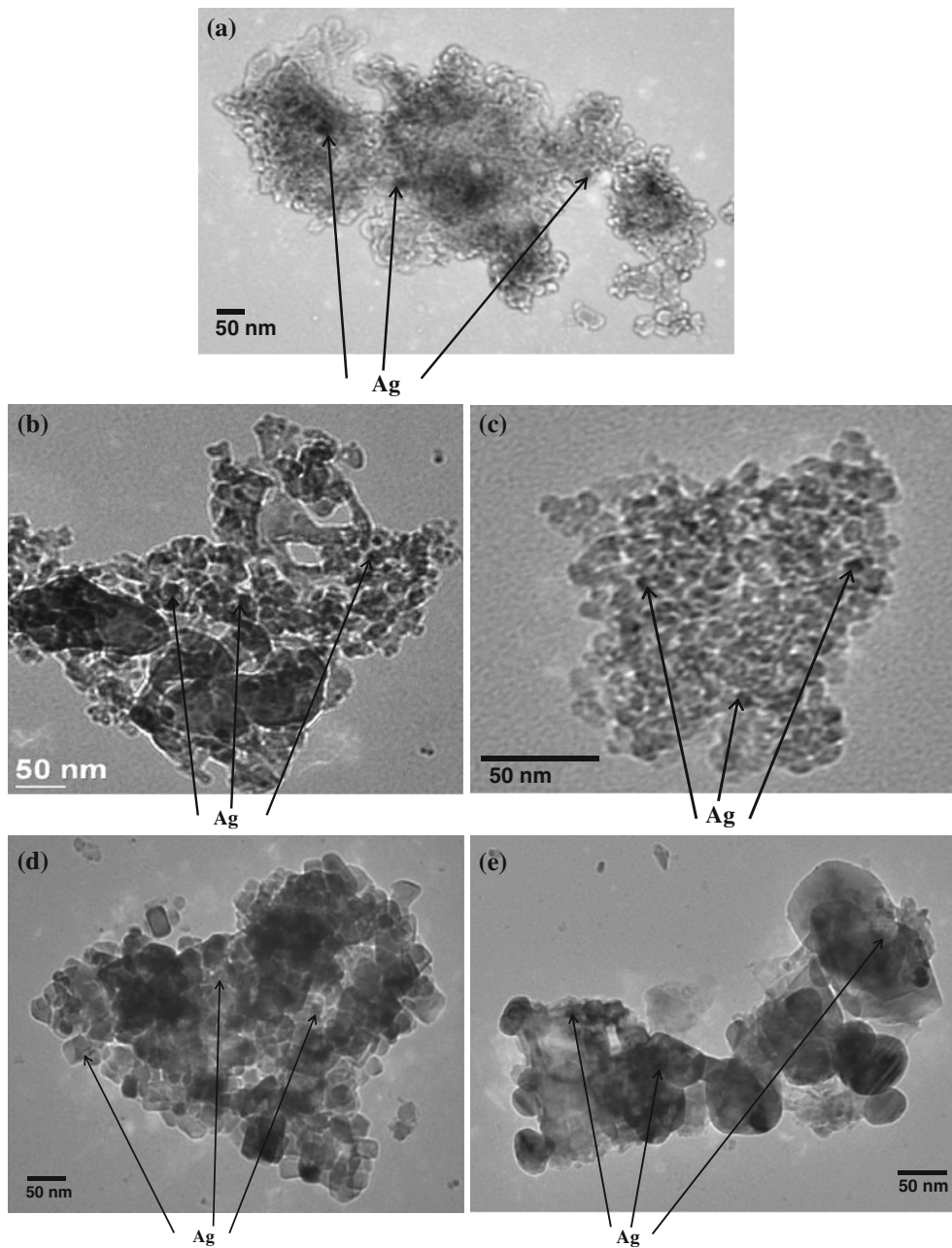


**Fig. 6** TEM-EDS images of **a** 14.7 wt% Ag/TiO<sub>2</sub>, **b** 17.3 wt% Ag/MgTiO<sub>3</sub>, **c** 17.0 wt% Ag/CaTiO<sub>3</sub>, **d** 17.2 wt% Ag/SrTiO<sub>3</sub>, and **e** 17.1 wt% Ag/BaTiO<sub>3</sub> catalysts (before the reaction)

**Table 3** TPD results of O<sub>2</sub> of studied Ag-loaded catalysts on different supports at their optimum Ag loadings

Support	Optimum Ag loading (wt%)	O <sub>2</sub> uptake ( $\mu\text{mol g}^{-1}$ )	C <sub>2</sub> H <sub>4</sub> uptake ( $\mu\text{mol g}^{-1}$ )
TiO <sub>2</sub>	14.7	367	944
MgTiO <sub>3</sub>	17.3	812	4,564
CaTiO <sub>3</sub>	17.0	405	4,721
SrTiO <sub>3</sub>	0	3,636	5,914
SrTiO <sub>3</sub>	17.2	5,155	6,308
BaTiO <sub>3</sub>	17.1	3,092	5,398

was the optimum support calcination temperature for the SrTiO<sub>3</sub> support (and other supports, except TiO<sub>2</sub>) was applied for all supports at various Ag loadings to compare the catalytic activity.

### 3.2.2 Effect of Nanocrystalline Perovskite Titanate Type

To compare SrTiO<sub>3</sub> with all the other perovskite titanate and TiO<sub>2</sub> supports for the ethylene epoxidation reaction performance, all the supports were calcined at 923 K with different Ag loadings. Figure 9 shows the ethylene epoxidation

**Fig. 7** Deconvoluted Ag 3d XPS peaks of 17.2 wt% Ag/SrTiO<sub>3</sub> **a** before the reaction and **b** after the reaction

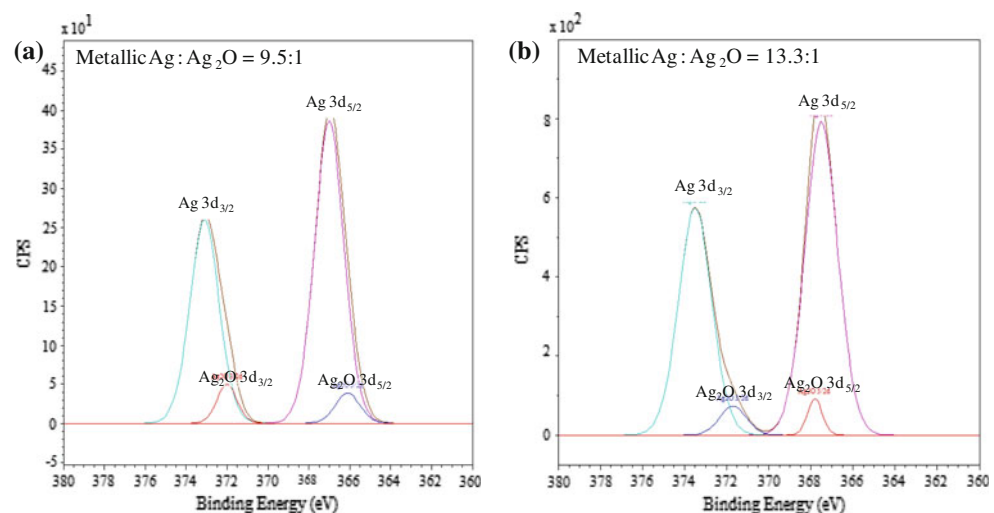


**Table 4** Coke formation on spent Ag-loaded catalysts after 6 h on stream of the ethylene epoxidation reaction (6 % O<sub>2</sub> and 6 % C<sub>2</sub>H<sub>4</sub> balanced with He, a space velocity of 6,000 h<sup>-1</sup>, a pressure of 24.7 psia, and a reaction temperature of 548 K)

Support	Optimum Ag loading (wt%)	Coke formation at 6 h (wt%)	Coke formation at 48 h (wt%)
$\alpha$ -Al <sub>2</sub> O <sub>3</sub>	14.9	4.3	9.8
TiO <sub>2</sub>	14.7	6.7	13.2
MgTiO <sub>3</sub>	17.3	9.2	15.7
CaTiO <sub>3</sub>	17.0	7.0	14.1
SrTiO <sub>3</sub>	17.2	3.3	4.5
BaTiO <sub>3</sub>	17.1	2.5	6.9

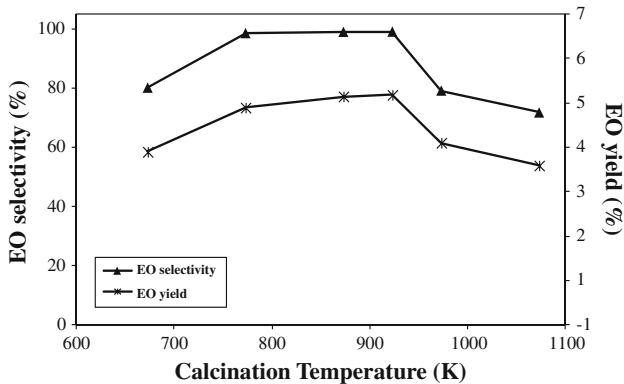


**Fig. 8** EO yield and EO selectivity as a function of SrTiO<sub>3</sub> support calcination temperatures (6 % O<sub>2</sub> and 6 % C<sub>2</sub>H<sub>4</sub> balanced with He, a space velocity of 6,000 h<sup>-1</sup>, a pressure of 24.7 psia, Ag loading of 17.2 wt%, a reaction temperature of 548 K and reaction time of 6 h)

performance as a function of reaction temperature over different supports with their own optimum Ag loadings. For any given support of the Ag catalyst, the EO yield increased as the reaction temperature increased from 498 to 548 K and reached a maximum at 548 K. When the reaction

temperature was raised from 548 to 563 K, the EO yield was significantly lowered. For any given support of the Ag catalyst, the EO selectivity tended to decrease considerably with increasing reaction temperature, except for the 17.2 wt% Ag/SrTiO<sub>3</sub> catalyst which remained relatively high in the temperature range of 498 to 548 K. The reason for the decline of catalytic activity at high temperatures is the large increment of the complete oxidation to CO<sub>2</sub> at a higher temperature [41, 44]. The catalytic activity of the Ag catalysts on all nanocrystalline cubic perovskite titanate supports (Ag/CaTiO<sub>3</sub>, Ag/SrTiO<sub>3</sub>, and Ag/BaTiO<sub>3</sub> catalysts), except Ag/MgTiO<sub>3</sub> catalyst were higher than that on the Ag/TiO<sub>2</sub> catalyst, suggesting that the incorporation of proper alkaline earth metals (Ca, Sr, and Ba) in the perovskite titanate supports can enhance the catalytic performance towards the ethylene epoxidation reaction. The best catalyst for ethylene epoxidation is the 17.2 wt% Ag/SrTiO<sub>3</sub> catalyst, providing a maximum EO yield of 4.7 % and the highest EO selectivity of 99.12 % at the reaction temperature of 548 K. These results can be well correlated to the TPD results of oxygen and ethylene of this catalyst, showing the highest oxygen adsorption capacity with a relatively high ethylene uptake as compared with other catalysts. However, when the Ag loading increased from 17.2 to 19.8 wt%, the EO selectivity and yield decreased even though the oxygen adsorption capacity increased. The results suggest that the ability of oxygen to adsorb onto the catalyst is not the sole factor affecting the ethylene epoxidation activity. As the Ag loading increases, the Ag particle size becomes larger. Too small or too large Ag particle sizes exhibit a negative effect towards the reaction [45, 46]. The large fraction of metallic Ag (Fig. 7) in this catalyst also provides a positive effect for the epoxidation reaction [46]. The 17.1 wt% Ag/BaTiO<sub>3</sub> catalyst had secondly high EO yield with lower EO selectivity among the titanates. This catalyst also possesses the second highest capability of adsorbing and desorbing O<sub>2</sub> (the reactant of the

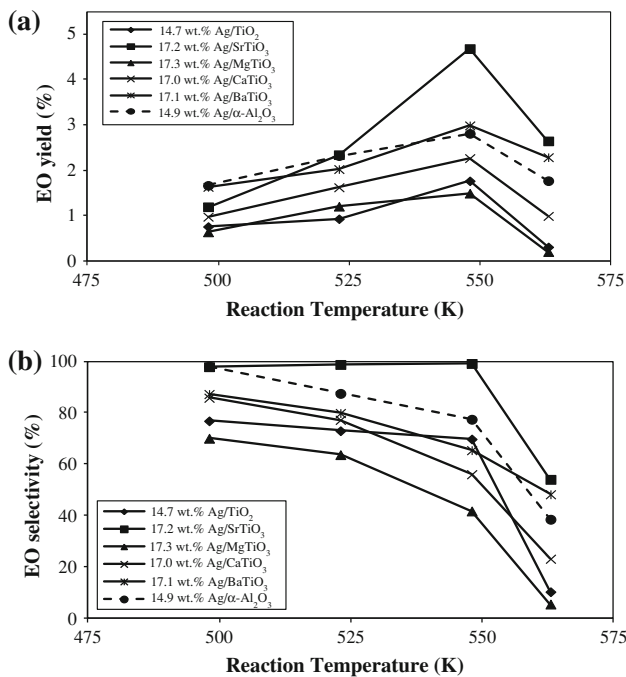


**Fig. 9** **a** EO yield and **b** EO selectivity as a function of reaction temperatures on various Ag-based perovskite titanate catalysts compared with a commercial Ag/α-Al<sub>2</sub>O<sub>3</sub> catalyst and Ag/TiO<sub>2</sub> catalyst (6 % O<sub>2</sub> and 6 % C<sub>2</sub>H<sub>4</sub> balanced with He, a space velocity of 6,000 h<sup>-1</sup>, a pressure of 24.7 psia, and a support calcination temperature of 923 K)

epoxidation reaction). As a consequence, the selective oxidation reaction could be easily facilitated, leading to higher ethylene oxide production performance. The lowest catalytic performance was found on the 17.3 wt% Ag/MgTiO<sub>3</sub> catalyst. The low oxygen adsorption capacity with the highest amount of Ag<sub>2</sub>O (the lowly active oxide species) is the reason for the inferior performance of the Ag/MgTiO<sub>3</sub> catalyst. Furthermore, the Ag<sub>2</sub>O, the lowly active oxide species that easily forms on small Ag particles, decreases the epoxidation rate [47]. The presence of this lowly active oxide species might be associated with the low EO selectivity in Ag/MgTiO<sub>3</sub> and Ag/BaTiO<sub>3</sub> catalysts in the way that the undesired reaction pathways might have faster reaction rates than the epoxidation rate, leading to more undesired products. The TEM results showed that the average Ag particle sizes slightly increased from 59.4 to 64 nm after the ethylene epoxidation reaction, pointing out a small extent of sintering of the catalyst during the reaction.

All results indicate that the epoxidation of ethylene depends on the support type, specific surface area, Ag loading, reaction temperature, oxygen adsorption capacity, Ag particle size, and the ratio of metallic Ag to Ag<sub>2</sub>O of the catalysts. The best catalyst for the selective oxidation of ethylene was 17.2 wt% Ag-loaded on a SrTiO<sub>3</sub> support

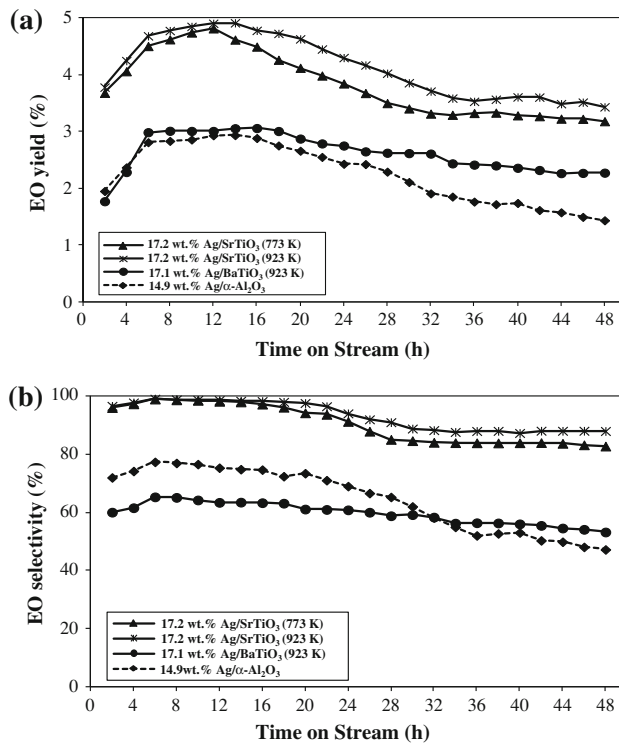


**Fig. 10** EO yield (a) and EO selectivity (b) as a function of time on stream for 17.2 wt% Ag/SrTiO<sub>3</sub> catalyst at the support calcination temperatures of 773 and 923 K compared with 17.1 wt% Ag/BaTiO<sub>3</sub> catalyst and a commercial 14.9 wt% Ag/α-Al<sub>2</sub>O<sub>3</sub> catalyst (6 % O<sub>2</sub> and 6 % C<sub>2</sub>H<sub>4</sub> balanced with He, a space velocity of 6,000 h<sup>-1</sup>, a pressure of 24.7 psia, and a reaction temperature of 548 K)

with a support calcination temperature of 923 K, large Ag particle sizes of about 59 nm, a low specific surface area of 1.5 m<sup>2</sup>/g, and the highest oxygen adsorption capacity of 5,155 μmol/g. Moreover, it can be concluded that the incorporation of an Sr atom in the TiO<sub>2</sub> support with the nanocrystalline structure plays an important role in the superior catalytic performance as a catalyst support for the Ag catalyst towards the ethylene epoxidation reaction.

The long-term stability in terms of EO yield and EO selectivity as a function of time on stream of the optimum 17.2 wt% Ag/SrTiO<sub>3</sub> catalyst (prepared at a support calcination temperature of 923 K) was compared with the same catalyst (prepared at support calcination temperature of 773 K), the 17.1 wt% Ag/BaTiO<sub>3</sub> catalyst (which provided the second place of activity in the group of titanate catalysts) and the 14.9 wt% Ag/commercial α-Al<sub>2</sub>O<sub>3</sub> catalyst. As shown in Fig. 10, the optimum 17.2 wt% Ag/SrTiO<sub>3</sub> catalyst exhibits the longest catalytic stability, providing a steady EO yield of 3.53 % after 36 h of operation as compared to 4.68 % at 6 h of operation and a steady EO selectivity of about 88 % as compared to 99.12 % at 6 h of operation. The similar trends of the drop in the catalytic activities were found for all catalysts.

Interestingly, the 14.9 wt% Ag/commercial  $\alpha$ -Al<sub>2</sub>O<sub>3</sub> catalyst showed the worst long-term stability, giving the lowest in both EO yield of 1.91 and 58 % of EO selectivity after 32 h of operation with a significant drop in the catalytic activity after 48 h of operation. The decreases in catalytic activities of all catalysts resulted from coke formation. The lower the coke formation, the lower the decrease in long-term stability of the catalyst (Table 4). It can be concluded that the 17.2 wt% Ag/SrTiO<sub>3</sub> catalyst with the support calcination temperature of 923 K is the most effective catalyst for the ethylene epoxidation reaction, giving not only the highest EO yield and EO selectivity but also providing the highest long-term stability.

## 4 Conclusions

The support calcination temperature has a significant effect on the physical and textural properties of the catalysts. The optimum calcination temperature of the support was 923 K. Among the various Ag-loaded nanocrystalline titanate catalysts, the 17.2 wt% Ag/SrTiO<sub>3</sub> catalyst exhibited the best catalytic activity to produce ethylene oxide, providing the highest EO yield of 4.7 % with enhanced EO selectivity to 99.12 % at the reaction temperature of 548 K. The superior catalytic activity of the 17.2 wt% Ag/SrTiO<sub>3</sub> catalyst may correspond to the moderate Ag particle sizes [48] and higher oxygen adsorption ability.

**Acknowledgments** This work was supported by The Royal Golden Jubilee Ph.D. Program (RGJ-Industry) awarded by The Thailand Research Fund with the in-kind support from PTT Global Chemical Public Co. Ltd.; the Sustainable Petroleum and Petrochemicals Research Unit, Center of Excellence on Petrochemical and Materials Technology, Chulalongkorn University (Thailand); and the Transportation Energy Center, Department of Chemical Engineering, University of Michigan (USA).

## References

1. Lefort TE (1935) US Patent 1:998
2. Marta CN, Amorim DC, Fabio BP, Schmal M (2007) *J Catal* 248:124–129
3. Jankowiak JT, Barteau MA (2005) *J Catal* 236:366–378
4. Santen RAV, Kuipers HPCE (1987) *Adv Catal* 35:1–57
5. Bharthwaj A (2002) Ph.D. Dissertation. Massachusetts Institute of Technology, USA
6. Minahan DM, Hoflund GB, Epling WS, Schoenfeldz DW (1997) *J Catal* 168:393–399
7. Peng Y, Zhang S (1992) *Catal Lett* 12:307–318
8. Daniel T, Francesc I, Lambert RM (2008) *J Catal* 260:380–383
9. Frank ER, Hamers RJ (1997) *J Catal* 172:406–413
10. Karavasilis Ch, Bebelis S, Vayenas CG (1996) *J Catal* 160: 205–213
11. Grant RB, Lambert RM (1985) *Langmuir* 1:29–33
12. Zhou XG, Yuan WK (2005) *Chem Eng Process* 44:1098–1107
13. Dellamorte JC, Lauterbach J, Barteau MA (2007) *Catal Today* 120:182–185
14. Podgornov EA, Prosvirin IP, Bukhtiyarov VI (2000) *J Mol Catal* 158:337–343
15. Yeung KL, Gavriliidis A, Varma A, Bhasiny MM (1998) *J Catal* 174:1–12
16. Lafarga D, Varma A (2000) *Chem Eng Sci* 55:749–758
17. Ayame A, Uchida Y, Ono H, Miyamoto M, Sato T, Hayasaka H (2003) *Appl Catal A* 244:59–70
18. Fotopoulos AP, Triantafyllidis KS (2007) *Catal Today* 127: 148–156
19. Korchagin AI, Kuksanov NK, Lavrukhan AV, Fadeev SN, Salimov RA, Bardakhanov SP, Goncharov VB, Suknev AP, Paukshtis EA, Larina TV, Zaikovskii VI, Bogdanov SV, Balzhinimaev BS (2005) *Vacuum* 77:485–491
20. Wolf A, Schuth F (2002) *Appl Catal A* 226:1–13
21. Eldridge JM, Ahn KY, Forbes L (2009) US Patent 2:1–35
22. Kim YC, Park NC, Shin JS, Lee SR, Lee YJ, Moon DJ (2003) *Catal Today* 87:153–162
23. Epifani M, Giannini C, Tapfer L, Vasanelli L (2000) *J Am Ceram Soc* 83:2385–2393
24. Sreethawong T, Suzuki Y, Yoshikawa S (2005) *J Solid State Chem* 178:329–338
25. Puangpitch T, Sreethawong T, Yoshikawa S, Chavadej S (2008) *J Mol Catal A: Chem* 287:70–79
26. Puangpitch T, Sommakkettarin P, Chavadej S, Sreethawong T (2010) *Int J Hydrogen Energy* 35:12428–12442
27. Chongtertoonskul A, Schwank JW, Chavadej S (2012) *J Mol Catal A: Chem* 358:58–66
28. Sreethawong T, Suzuki Y, Yoshikawa S (2005) *Int J Hydrogen Energy* 30:1053–1062
29. Sreethawong T, Yoshikawa S (2005) *Catal Commun* 6:661–668
30. Sreethawong T, Yoshikawa S (2006) *Int J Hydrogen Energy* 31:786–796
31. Sreethawong T, Puangpitch T, Chavadej S, Yoshikawa S (2007) *J Power Sources* 165:861–869
32. Sreethawong T, Laehsalee S, Chavadej S (2008) *Int J Hydrogen Energy* 33:5947–5957
33. Sreethawong T, Junbua C, Chavadej S (2009) *J Power Sources* 190:513–524
34. Puangpitch T, Sreethawong T, Yoshikawa S, Chavadej S (2009) *J Mol Catal A: Chem* 312:97–106
35. Puangpitch T, Chavadej S, Sreethawong T (2011) *Energy Convers Manage* 52:2256–2261
36. Cullity BD (1978) Elements of X-ray diffraction. Addison-Wesley, Reading
37. Jackson AG (1991) Handbook of crystallography. Springer, New York
38. Moulder JF, Stickle WF, Sobol PE, Bomben KD (1995) Handbook of X ray photoelectron spectroscopy: a reference book of standard spectra for identification and interpretation of XPS data. Physical Electronics, Eden Prairie
39. Chen S, Manos G (2004) *J Catal* 226:343–350
40. Brillas AA, Manos G (2003) *Catal Lett* 91:185–191
41. Rojuechai S (2006) Ph.D. Dissertation. The Petroleum and Petrochemical College, Chulalongkorn University, Bangkok, Thailand
42. Smith JV (1960) X-ray powder data file. American Society for Testing Materials, Philadelphia
43. Lin L, Lin W, Xie JL, Zhu YX, Zhao BY, Xie YC (2007) *Appl Catal B Environ* 75:52–58
44. Ozbek MO, Onal I, Santen RA (2011) *ChemCatChem* 3:150–153
45. Mastikhin VM, Goncharova SN, Tapilin VM, Terskikh VV, Balzhinimaev BS (1995) *J Mol Catal A: Chem* 96:175–179
46. Goncharova SN, Paukshtis EA, Balzhinimaev BS (1995) *Appl Catal A* 126:67–84
47. Lee JK, Verykios XE, Pitchai R (1989) *Appl Catal* 50:171
48. Hassani SS, Ghaseemi MR, Rashidzadeh M, Sobat Z (2009) *Cryst Res Cryst Technol* 44:948–952